Energy Proceedings
Vol 27, 2022
ISSN 2004-2965

Numerical Simulation of Fractured Enhanced Geothermal System Based on Projection-Based Embedded Discrete Fracture Model

Xiuwei Liu[1*], Shiqing Cheng[1], Dengke Shi[1], Dingning Cai[1], Fuguo Yin[1], Dawei Liu[1]

1 College of Petroleum Engineering, China University of Petroleum (Beijing), Beijing, China, 102249

* Corresponding Author at lxw19960606@163.com

ABSTRACT

Enhanced Geothermal System (EGS) is now the main method to extract heat from the hot dry rock, and the fractures are the key to achieving a high heat extraction. This paper extends the related transmissibility calculation method of non-neighboring connections (NNC) in the projection-based embedded discrete fracture model (pEDFM) to the calculation of effective thermal transmissibility. In this way, a thermal pEDFM is proposed to evaluate the heat extraction performance of the fractured EGS. The model verification is conducted by comparing the result of the thermal pEDFM and the analytical solution. At last, two simulation examples are utilized to illustrate the flexibility and the practicality of the thermal pEDFM, which reveals that the thermal pEDFM can be applied in the evaluation of the heat extraction analysis for the fractured EGS.

Keywords: Enhanced Geothermal System; Thermal pEDFM; Model verification; Two simulation examples

1. INTRODUCTION

Geothermal energy is a clean, renewable, and environmental-friendly energy resource and now is one of the alternatives to traditional fossil fuel energy [1]. According to the statistics, the stored geothermal energy worldwide is about 1.3×10^{27}J, which is enough to meet the energy demand of human society for more than 200 million years [2]. The majority of geothermal energy is stored in the hot dry rock buried 3-10 km beneath the ground [3], and the popular exploration method is the enhanced geothermal system (EGS) which creates new fractures or re-opens the existing fractures to generate the main heat extraction channels for the injected fluid [4].

Many studies have been down for the numerical simulation of fractured EGS. Zhao et al [5] put forward a three-dimensional thermal-hydro-mechanical for the simulation of the fractured EGS with the 50K/km temperature gradient and 6250-6750m buried depth. Hofmann et al [6] built a two-dimension EGS model to simulate the heat extraction performance. They made a comparison between complex fracture networks and parallel fractures and found that a complex fracture network is more beneficial for EGS. Pandey et al [7] simulated a 2D EGS with a single fracture based on the finite element method and local grid refinement (LGR), and they studied how the variation of fracture aperture affected the production temperature of EGS. Qu et al [8] studied the influence of fracture morphology on the production performance of EGS based on COMSOL. They concluded that the numbers and the complexity of fractures are favorable for high production performance, but the width of branch fractures had little effect. Song et al [9] first proposed a multilateral wells EGS model and compared the heat extraction performance of multilateral wells with double wells. They demonstrated that the multilateral wells EGS model has a more pronounced performance. Ma et al [10] made a multi-well injection EGS with a leaf-like bifurcated fracture network based on fractal and bifurcation theory. They found that a higher fracture bifurcation level and bifurcation length ratio are necessary. Zhou et al [11] did research on the influence of randomly distributed fracture aperture on EGS performance through a 2D numerical model and the coefficient of variation. Their simulation results revealed that a higher mean aperture could make a promotion in the production temperature.

The aforementioned studies are meaningful to the simulation of fractured EGS, but the fracture models in these studies are all based on the LGR method or discrete fracture model (DFM). The application of these two methods will cause prohibitive computational costs due to large-scale grid meshing when there are many intersecting fractures. Embedded discrete fracture model (EDFM) is an appealing method for efficiently modeling fluid flow between the matrix and the fractures based on the transmissibility of the non-neighboring connections (NNC). It was firstly proposed by Lee et al

[12], and then got rapid development in the oil and gas seepage simulation in the petroleum industry (Moinfar et al [13], Xu et al [14]). Recently, many researchers have developed EDFM for the simulation of fractured EGS. Sun et al [15] extended EDFM to thermal EDFM, and they affirmed the reliability of thermal EDFM by comparing it with the LGR method. They also presented an example of fractured EGS with two horizontal wells. Yu et al [16] coupled EDFM with geomechanics to make a thermal-hydraulic-mechanics simulation for geothermal reservoir simulation. However, Tene et al [17] and Jiang et al [18] discussed the disadvantage of EDFM and improved it into a projection-based embedded discrete fracture model (pEDFM). Hereafter, Olorode et al [19] presented the first 3D pEDFM algorithm and simulation cases.

In this paper, we develop the calculation method of effective thermal transmissibility of NNC in pEDFM based on the origin algorithm of the transmissibility. A thermal pEDFM is put forward to simulate the fractured EGS. The related model verification and simulation examples demonstrate the reliability and practicality of this research, which enrich the simulation method and calculation efficiency of fractured EGS.

2. THEORY

2.1 Governing equations

Before presenting the governing equations, the following assumptions need to be assumed:

(1) The reservoir is homogeneous and isotropic; (2) The density, heat capacity, and heat conductivity of the fluid (water) and rock are constant; (3) The fluid flowing in the matrix and fracture obeys Darcy law; (4) Local thermal equilibrium is assumed; (5) Single-phase fluid (water) and the fluid will not vaporize.

2.1.1 Mass balance equation

For the matrix system

$$\frac{\partial\left(\rho_f\phi\right)_m}{\partial t}-\nabla\cdot\left(\rho_f\frac{k}{\mu}\nabla p\right)_m= \left(\rho_f q_f\right)_m+\sum q_{m,F} \tag{1}$$

For the fracture system

$$\frac{\partial\left(\rho_f\phi\right)_F}{\partial t}+\nabla\cdot\left(\rho_f\rho_f\frac{k}{\mu}\nabla p\right)_F= \left(\rho_f q_f\right)_F+\sum q_{m,F}+\sum q_{F,F} \tag{2}$$

where ρ_f is the fluid density, ϕ is the porosity, k is the permeability, μ is the viscosity, p is the pressure, q_f is the source/sink item, $q_{m,F}$ is the flux exchange between the matrix and fracture, $q_{F,F}$ is the flux exchange between the fracture and fracture, subscript m and F represent the matrix and fracture.

2.1.2 Energy balance equation

For the matrix system

$$\frac{\partial\left(\left(\rho U\right)_{eff}T\right)_m}{\partial t}-\nabla\cdot\left(\rho_f\frac{k}{\mu}h_f\nabla p\right)_m -\nabla\cdot\left(\lambda_{eff}\nabla T\right)_m=\left(\rho_f q_f h_f\right)_m+\sum E_{m,F} \tag{3}$$

For the fracture system

$$\frac{\partial\left(\left(\rho U\right)_{eff}T\right)_F}{\partial t}-\nabla\cdot\left(\rho_f\frac{k}{\mu}h_f\nabla p\right)_F -\nabla\cdot\left(\lambda_{eff}\nabla T\right)_F=\left(\rho_f q_f h_f\right)_F+\sum E_{m,F}+\sum E_{F,F} \tag{4}$$

where

$$\left(\rho U\right)_{eff}=\left(1-\phi\right)\rho_s c_{ps}+\phi\rho_f c_{pf}$$

$$\lambda_{eff}=\left(1-\phi\right)\lambda_s+\phi\lambda_f$$

In the above equations, ρ_s is the rock density, c_{ps} and c_{pf} are the heat capacity of rock and fluid, λ_s and λ_f are the heat conductivity of rock and fluid, λ_{eff} is the effective thermal conductivity, h_f is the specific enthalpy of fluid, $E_{m,F}$ is the conductive heat exchange between the matrix and fracture, $E_{F,F}$ is the conductive heat exchange between the fracture and fracture.

2.2 Calculation of effective thermal conductivity in thermal pEDFM

For flowing problems, the key of pEDFM is the calculation of transmissibility of non-neighboring connections (NNC), the detailed definition of NNC, the projection rules, and the calculation method of transmissibility can be obtained by referring to the research of Olorode et al [19]. Here, for simplicity, only the calculation methods of effective thermal transmissibility of different NNC types are listed, by which a thermal pEDFM can be obtained. And this calculation is done during the preprocessing of the numerical simulation.

2.2.1 NNC type 1: Matrix-Fracture

The effective thermal transmissibility of this type can be calculated as

$$T_{th}^{NNC}=\frac{\lambda_{eff}^{NNC}A^{NNC}}{d^{NNC}} \tag{5}$$

where

$$A^{NNC}=2A_F$$

$$\lambda_{eff}^{NNC}=\frac{\left(\lambda_{eff}\right)_m\left(\lambda_{eff}\right)_F}{\left(\lambda_{eff}\right)_m+\left(\lambda_{eff}\right)_F}$$

$$d^{NNC}=\int_V dv/V$$

A_F is the fracture area, d^{NNC} is the average normal distance from the matrix to the fracture.

2.2.2 NNC type 2: Fracture-Fracture

In NNC type 2, the calculation method is the same as NNC type 1, but the corresponding parameters should be replaced by that of fracture segments.

2.2.3 NNC type 3: Intersecting Fracture

The calculation method is shown as

$$T_{th}^{NNC} = \frac{T_{th1}^{NNC} T_{th2}^{NNC}}{T_{th1}^{NNC} + T_{th2}^{NNC}} \tag{6}$$

where the half-effective thermal transmissibilities are

$$T_{th1}^{NNC} = \frac{\lambda_{eff1} \omega_1 L_{\text{int}}}{d_{F1}}$$

$$T_{th2}^{NNC} = \frac{\lambda_{eff2} \omega_2 L_{\text{int}}}{d_{F2}}$$

ω is the fracture width and L_{int} is the length of the intersection line between two fracture segments, d_F is the distance from the centroid of the fracture segment to the intersection line.

2.2.4 NNC type 4: Projection Matrix-Fracture

NNC type 4 refers to the connection between the projection matrix and the fracture, and

$$T_{th,pM-F}^{NNC} = \frac{\lambda_{eff,pM-F}^{NNC} A_P}{d_{pM-F}^{NNC}} \tag{7}$$

where A_p is the fracture projection area along each dimension, d_{NNC}^{pM-F} is the distance between the fracture segment centroid and projection cell centroid, and

$$\lambda_{eff,pM-F}^{NNC} = \frac{\left(\lambda_{eff}\right)_{pM} \left(\lambda_{eff}\right)_F}{\left(\lambda_{eff}\right)_{pM} + \left(\lambda_{eff}\right)_F}$$

2.2.5 NNC type 5: Projection Matrix-Matrix

The effective thermal transmissibility of NNC type 5 can be calculated as

$$T_{th,pM-M}^{NNC} = T_{th,M-M} \frac{A - A_P}{A} \tag{8}$$

where A is the whole area of the projection cell's face, $T_{th,M-M}$ is the matrix-matrix effective thermal transmissibility

$$T_{th,M-M} = \lambda_{eff} \frac{A}{\Delta L}$$

ΔL is the matrix cell size in each dimension.

2.3 Numerical simulation procedure

For numerical simulation, the governing equations are discretized by the finite volume method, and the whole procedure is conducted as *Fig.1*.

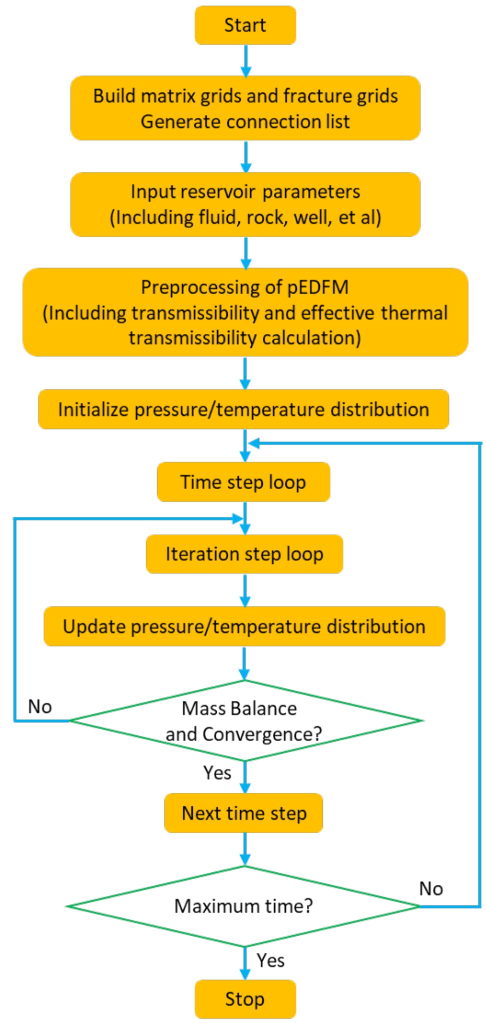

Fig.1 Schematic of the numerical simulation procedure

3. RESULTS

3.1 Model verification

Barends [20] derived an analytical solution for the fluid flow and heat transfer problem in a 2D matrix containing a single fracture in the infinite domain (*Fig.2*). The fluid is injected into the fracture at the velocity of u_{in}, and the temperature distributions in the fracture (T_f) and matrix (T_m) are respectively expressed as

$$T_F(x,t) = T_0 + \left(T_{in} - T_0\right) \cdot \\ erfc\left[\frac{\lambda_s x}{\rho_f c_{pf} u_{in} d} \sqrt{\frac{\rho_d c_{ps} u_{in}}{\lambda_s \left(u_{in} t + x\right)}}\right] \tag{9}$$

$$T_m(x,z,t) = T_0 + \left(T_{in} - T_0\right) \cdot \\ erfc\left[\frac{2\lambda_s x + |z| \rho_f c_{pf} u_{in} d}{\rho_f c_{pf} u_{in} d} \sqrt{\frac{\rho_s c_{ps} u_{in}}{\lambda_s \left(u_{in} t + x\right)}}\right] \tag{10}$$

where ρ is the density, λ is the heat conductivity, c_p is the heat capacity, d is the fracture width, x and z are the coordinates, T_0 and T_{in} are the initial temperature and the injection temperature, subscript f and s represent the fluid and rock.

In order to illustrate the reliability of the thermal pEDFM, a result comparison between this model and the analytical solution is carried out. A square calculation domain (100m×100m) is chosen, the relevant parameters are listed in *Table 1* and the whole simulation time is 300 days. Here, four scenarios are compared:

① The temperature profile in the fracture in 100d, 200d, and 300d;

② The temperature variation of three points along the fracture, including 20m, 40m, and 80m.

③ The temperature profile of the matrix at x = 4.5m in 100d, 200d, and 300d (*Fig.2*);

④ The temperature profile of the matrix at z = 1.5m in 100d, 200d, and 300d (*Fig.2*).

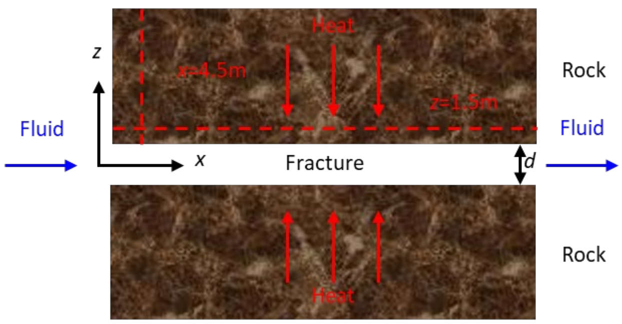

Fig.2 Schematic of the fluid flow and heat transfer problem in a 2D matrix containing a single fracture in the infinite domain

Table 1 The relevant parameters

Parameter	Value
Fluid density ρ_f	1000 kg/m^3
Fluid heat capacity c_{pf}	4200 J/(kg·K)
Rock density ρ_s	2700 kg/m^3
Rock heat capacity c_{ps}	1000 J/(kg·K)
Rock heat conductivity λ_s	2.8 W/(m·K)
Injection temperature T_{in}	303.15 K
Initial temperature T_0	353.15 K
Fracture width d	0.001 m
The velocity of injection u_{in}	0.01 m/s

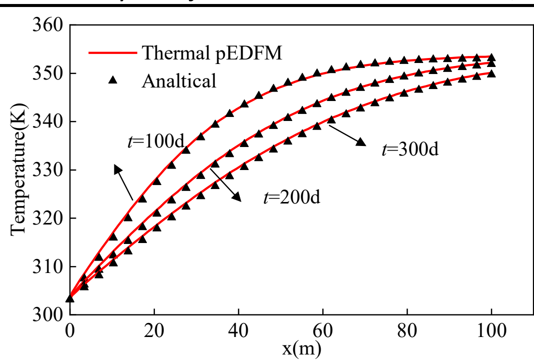

Fig.3 The temperature profile of fracture at different time

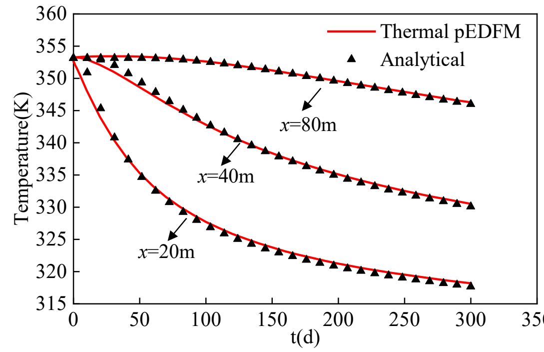

Fig.4 The temperature variation of different points along the fracture

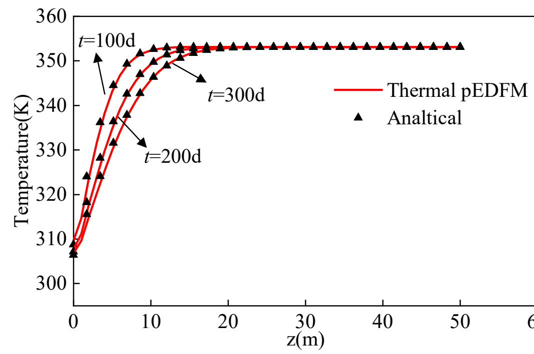

Fig.5 The matrix temperature profile at x = 4.5m

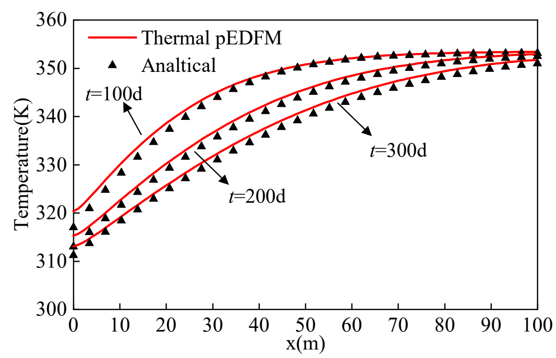

Fig.6 The matrix temperature profile at z = 1.5m

From *Fig.3* to *Fig.5*, it can be observed that the results of thermal pEDFM have a good coincidence with the analytical solution. In *Fig.6*, there exists a certain difference, but the whole error is within the acceptable range and this phenomenon is caused by the numerical discretization error. Therefore, the proposed thermal pEDFM is reliable and credible.

3.2 Simulation examples

In this section, two examples are modeled to further explain the flexibility and the practicality of the thermal pEDFM.

(1) Example 1

Example 1 is a 100m×100m×10m square domain with one injection well (lower-left corner of the domain) and one production well (upper right corner). There is a fracture between two wells (*Fig.7*). The whole simulation time is 10 years, and the rest of the relevant information is shown in Table 2.

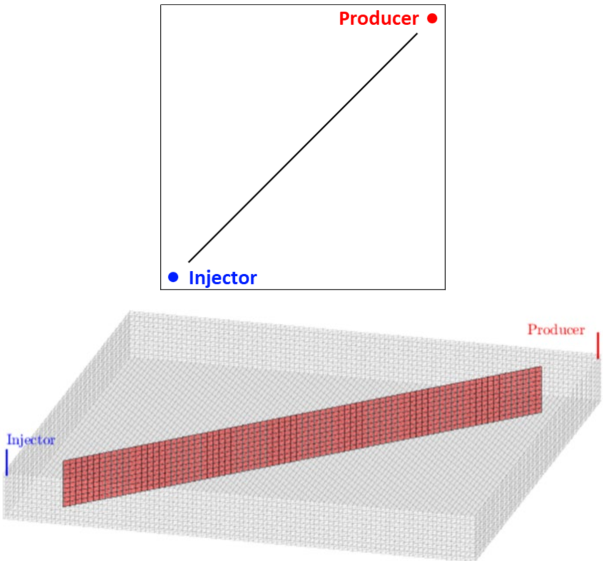

Fig.7 Schematic of example 1

Table 2 The relevant information of example 1

Parameter	Value
Fluid density ρ_f	1000 kg/m^3
Fluid heat capacity c_{pf}	4200 J/(kg·K)
Fluid heat conductivity λ_f	0.6 W/(m·K)
Rock density ρ_s	2700 kg/m^3
Rock heat capacity c_{ps}	1000 J/(kg·K)
Rock heat conductivity λ_s	2.8 W/(m·K)
Matrix permeability k_m	10^{-14} m^2
Fracture permeability k_F	10^{-10} m^2
Initial temperature	373.15 K
Initial pressure	10^7 Pa
Injection pressure	2×10^7 Pa
Injection temperature	293.15 K
Production pressure	10^7 Pa

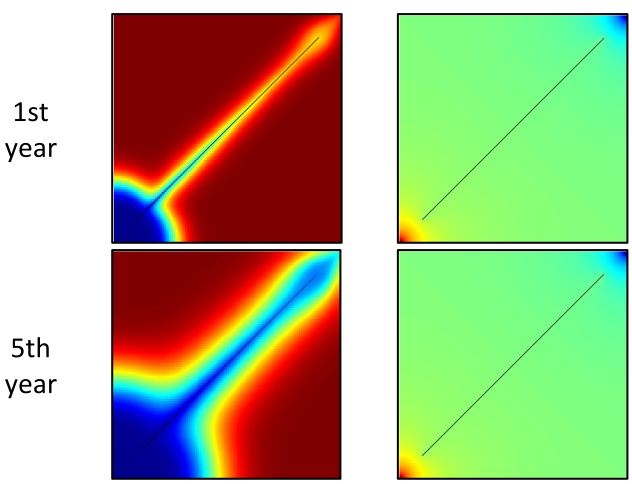

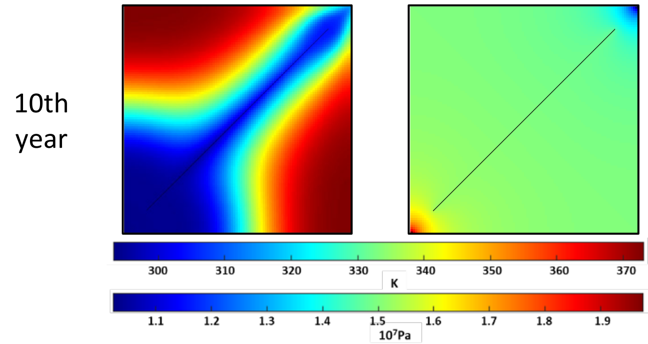

Fig.8 Temperature and pressure distribution of example 1 in 1st, 5th, and 10th year

Fig.8 shows the variation of temperature and pressure distribution at different times. It can be concluded that the injected cold water (293.15 K) moves to the production well due to the low-pressure gradient and makes heat exchange with the surrounding rock, which leads to the low-temperature front move too. After the 1st year, the low-temperature front reaches the fracture and quickly moves to the production well along the fracture, resulting in the thermal breakthrough in the production well. These phenomena illustrate that the fracture is the main channel for temperature propagation, and the entire heat extraction range is mainly distributed along the fracture. While, because the variation of physical properties of injection fluid is not considered, the pressure distribution remains unchanged in which the pressure around the injection well is about 2×10^7Pa and the pressure around the production well is about 10^7Pa.

(2) Example 2

Example 2 is based on example 1, the only difference is that there are 12 fractures (with a complex fracture network) between two wells (*Fig.9*).

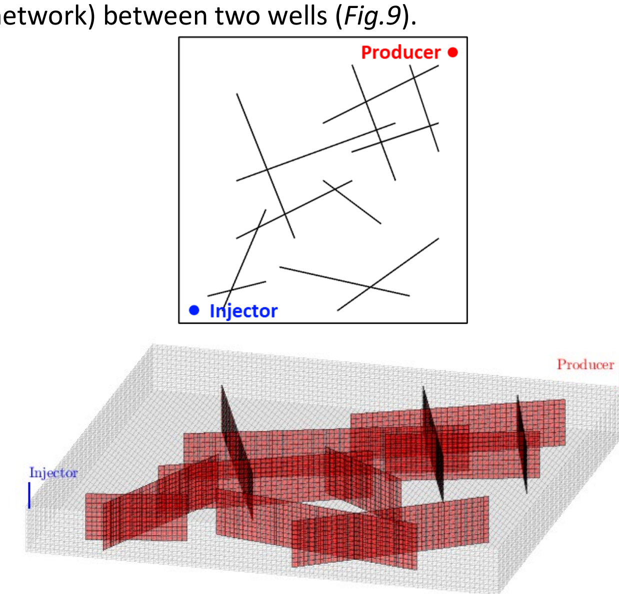

Fig.9 Schematic of example 2

Fig.10 illustrates the temperature and pressure field in the 1st, 5th, and 10th years. As time goes on, the low-temperature front moves along with the irregularly distributed fractures, and the fractures are still the main factor controlling the heat extraction area. Compared with Example 1, the fractures in example 2 have a bigger control range, which demonstrates that creating random fractures with a large control area is the key to obtaining a greater performance of the fractured EGS. Also, the pressure field is constant due to the unchanged physical properties of the injection fluid.

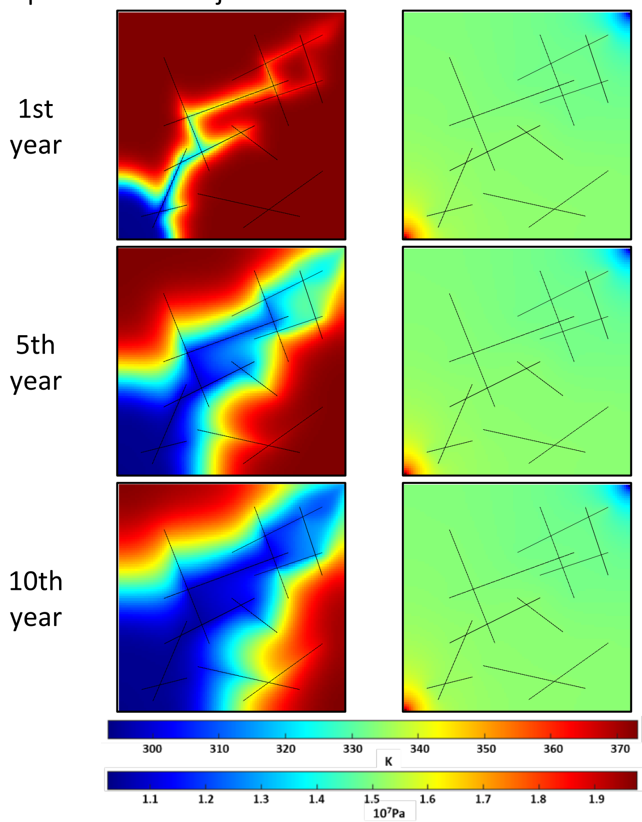

Fig.10 Temperature and pressure distribution of example 2 in 1st, 5th, and 10th year

(3) Comparison of production temperature of Example 1 and Example 2

In *Fig.11*, the production temperature of Example 1 and Example 2 both have two stages: stable stage and declining stage. But the stable time of Example 1 (0.5 years) is about half of that of Example 2 (1 year). And after entering the declining stage, the decreasing rate of output temperature in Example 1 is much higher than that in Example2. This discrepancy ultimately leads to that the production temperature of Example 2 is overall bigger than that of Example 1. This is because the fracture system in Example 2 is more complex and when the injected cold water quickly moves along these fractures, the low-temperature front moves slowly towards the production well under the action of the complex fracture network, resulting in a long stable time in Example 2. Also, more fractures mean a bigger heat exchange area which makes a lower decreasing rate in Example 2. This phenomenon states that making a complex fracture network is a highly nontrivial factor.

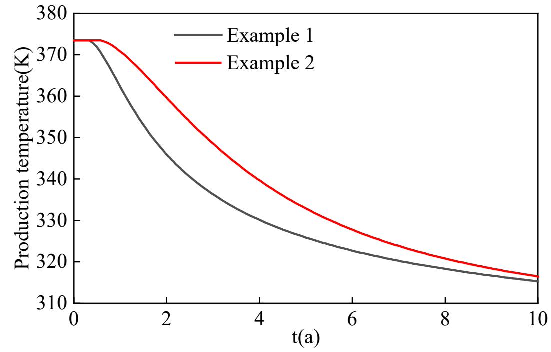

Fig.11 Production temperature comparison between Example 1 and Example 2

4. CONCLUSIONS

(1) The transmissibility calculation method of NNC in pEDFM is extended to the effective thermal conductivity, which forms a thermal pEDFM for the simulation of fractured EGS.

(2) By the contrast of calculation results between thermal pEDFM and analytical solution, the reliability of this proposed model is demonstrated.

(3) Simulation examples reveal the practicality of the thermal pEDFM and affirm that the fracture is the main flow channel of injection fluid and controls the heat extraction area. A complex fracture network is beneficial for the heat extraction performance of fractured EGS.

ACKNOWLEDGEMENT

We appreciate that the MRST platform provides the source code based on which we can make secondary development.

REFERENCE

[1] Salimzadeh S, Nick H M, Zimmerman R W. Thermoporoelastic effects during heat extraction from low-permeability reservoirs[J]. Energy, 2018, 142: 546-558.

[2] Lu S M. A global review of enhanced geothermal system (EGS)[J]. Renewable and Sustainable Energy Reviews, 2018, 81: 2902-2921.

[3] Brown D. The US hot dry rock program-20 years of experience in reservoir testing[C]. Proceedings of the world geothermal congress, Florence, Italy. 1995.

[4] Chamorro C R, García-Cuesta J L, Mondéjar M E, et al. Enhanced geothermal systems in Europe: An estimation and comparison of the technical and sustainable potentials[J]. Energy, 2014, 65: 250-263.

[5] Zhao Y, Feng Z, Feng Z, et al. THM (Thermo-hydro-mechanical) coupled mathematical model of fractured media and numerical simulation of a 3D

enhanced geothermal system at 573 K and buried depth 6000–7000 M[J]. Energy, 2015, 82: 193-205.
[6] Hofmann H, Babadagli T, Yoon J S, et al. A hybrid discrete/finite element modeling study of complex hydraulic fracture development for enhanced geothermal systems (EGS) in granitic basements[J]. Geothermics, 2016, 64: 362-381.
[7] Pandey S N, Chaudhuri A, Kelkar S. A coupled thermo-hydro-mechanical modeling of fracture aperture alteration and reservoir deformation during heat extraction from a geothermal reservoir[J]. Geothermics, 2017, 65: 17-31.
[8] Qu Z, Zhang W, Guo T. Influence of different fracture morphology on heat mining performance of enhanced geothermal systems based on COMSOL[J]. International Journal of Hydrogen Energy, 2017, 42(29): 18263-18278.
[9] Song X, Shi Y, Li G, et al. Numerical simulation of heat extraction performance in enhanced geothermal system with multilateral wells[J]. Applied energy, 2018, 218: 325-337.
[10] Ma Y, Li S, Zhang L, et al. Analysis on the heat extraction performance of multi-well injection enhanced geothermal system based on leaf-like bifurcated fracture networks[J]. Energy, 2020, 213: 118990.
[11] Zhou D, Tatomir A, Niemi A, et al. Study on the influence of randomly distributed fracture aperture in a fracture network on heat production from an enhanced geothermal system (EGS)[J]. Energy, 2022, 250: 123781.
[12] Lee S H, Lough M F, Jensen C L. Hierarchical modeling of flow in naturally fractured formations with multiple length scales[J]. Water resources research, 2001, 37(3): 443-455.
[13] Moinfar A, Varavei A, Sepehrnoori K, et al. Development of a novel and computationally-efficient discrete-fracture model to study IOR processes in naturally fractured reservoirs[C]. SPE improved oil recovery symposium, Tulsa, Oklahoma, 2012.
[14] Xu Y, Sepehrnoori K. Development of an embedded discrete fracture model for field-scale reservoir simulation with complex corner-point grids[J]. SPE Journal, 2019, 24(04): 1552-1575.
[15] Sun H, Yu W, Wu K, et al. A powerful thermal-EDFM for modeling enhanced geothermal system with 3D complex fracture networks[C]. 55th US Rock Mechanics/Geomechanics Symposium. Virtual, 2021.
[16] Yu X, Winterfeld P, Wang S, et al. A geomechanics-coupled embedded discrete fracture model and its application in geothermal reservoir simulation[C]. SPE Reservoir Simulation Conference. Galveston, Texas, USA, 2019.
[17] Ţene M, Bosma S B M, Al Kobaisi M S, et al. Projection-based embedded discrete fracture model (pEDFM)[J]. Advances in Water Resources, 2017, 105: 205-216.
[18] Jiang J, Younis R M. An improved projection-based embedded discrete fracture model (pEDFM) for multiphase flow in fractured reservoirs[J]. Advances in water resources, 2017, 109: 267-289.
[19] Olorode O, Wang B, Rashid H U. Three-dimensional projection-based embedded discrete-fracture model for compositional simulation of fractured reservoirs[J]. SPE Journal, 2020, 25(04): 2143-2161.
[20] Barends F B. Complete solution for transient heat transport in porous media, following Lauwerier's concept[C]. SPE annual technical conference and exhibition. Florence, Italy, 2010.